SWARM ABSOLUTE SCALAR AND VECTOR MAGNETOMETER BASED ON HELIUM 4 OPTICAL PUMPING

Jean-Michel Leger[(1)], François Bertrand[(1)], Thomas Jager[(1)], Matthieu Le Prado[(1)], Isabelle Fratter[(2)], Jean-Claude Lalaurie[(2)]

[(1)]CEA, LETI, MINATEC,
F38054 Grenoble, France
Email : jean-michel.leger@cea.fr

[(2)]Centre National d'Etudes Spatiales
18 Avenue Edouard Belin, 31401 Toulouse Cedex 9, France
Email : isabelle.fratter@cnes.fr

INTRODUCTION

The Absolute Scalar Magnetometer (ASM) developed by CEA-LETI in partnership with CNES is an optically pumped ^{4}He magnetometer which shall provide absolute scalar measurements of the magnetic field with high accuracy and stability for the calibration of the Vector Field Magnetometer (VFM) developed by the Danish National Space Center. In addition and on an experimental basis the ASM will be able to operate as a vector field magnetometer. Both operating principle and related performances are detailed in the following paragraphs.

ASM OPERATING PRINCIPLE

Scalar field measurement

The ASM is an optically pumped ^{4}He magnetometer based on an electronic magnetic resonance whose effects are amplified by a laser pumping process [1-2], as detailed on Fig. 1. A fraction of the atoms of a ^{4}He gaz cell are first excited to the 2^3S_1 metastable state by means of a high frequency discharge. This energy level is split by the static magnetic field B_0 into three Zeeman sublevels. As the energy gap ΔE between the levels is directly proportional to the ambient scalar field B_0, its determination allows the measurement of B_0 (1).

$$\Delta E = \gamma \hbar B_0 \qquad \text{where } \gamma \text{ is the } ^4\text{He gyromagnetic ratio for the } 2^3S_1 \text{ state [3]} \tag{1}$$

The measurement of B_0 is then performed by exciting and detecting the paramagnetic resonance between the Zeeman sublevels. To generate the resonance an oscillating radiofrequency field B_1 is applied on the ^{4}He gaz cell: when its frequency matches the Larmor frequency of the Zeeman sublevels ($\omega_0 = \gamma B_0$) the magnetic resonance occurs and transitions are induced between the sublevels.

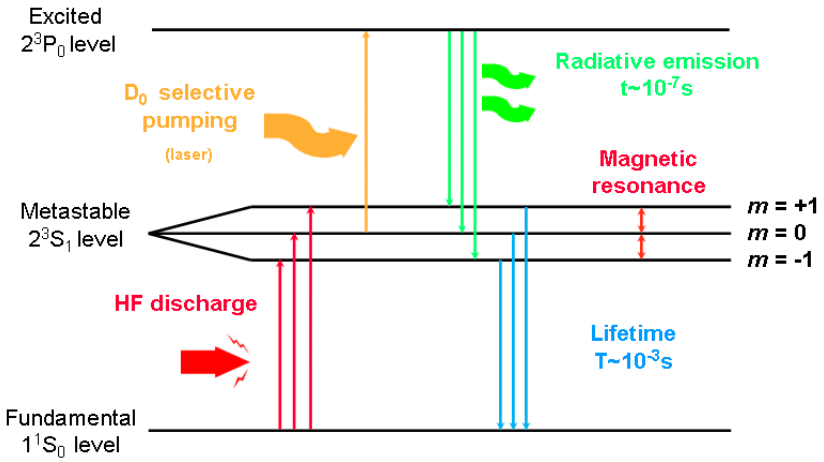

Fig. 1. ^{4}He energy diagram and ASM principle of operation

However, at thermal equilibrium the sublevels are almost equally populated and no significant change induced by the resonance can be detected. To finally enhance and detect the resonance, a selective pumping from one of the Zeeman sublevel to the 2^3P_0 state is performed thanks to a frequency tuned linearly polarized laser light. The resulting disequilibrium between the Zeeman sublevels populations improves the resonance signal amplitude by several orders of magnitude while the monitoring of the intensity of the laser light transmitted through the ^{4}He cell allows its detection.

Vector field measurement

The ASM magnetometer can also provide a vector measurement of the magnetic field using the information provided by the superimposition of 3 low frequency orthogonal magnetic fields onto the B_0 field seen by the ^{4}He sensing cell (2).

$$\left\| \vec{B}_{tot} \right\| = \left\| \vec{B}_0 + \sum_{j=1}^{3} \beta^j \cos(\omega_j t) \vec{e}_j \right\| \tag{2}$$

The vector measurement is simply obtained by processing the scalar output measurement containing the principal harmonics at the ω_j pulsations. The vector field reconstruction in the ASM reference frame is finally achieved thanks to a specific calibration process [2] from which the vector modulation amplitudes β_j and their respective orientations $\boldsymbol{e}_j$ in the ASM frame are derived.

ASM HARDWARE ARCHITECTURE

To take full advantage of the scalar magnetometer performances we defined an architecture that is free of the orientation effects common to all standard scalar magnetometers based on magnetic resonance. Each of the following processes has to be taken into account to guarantee the sensor isotropy:

- the distribution of atoms on the three sublevels 2^3S_1 resulting from optical pumping cycle is directly depending on the relative orientation θ_F between the static magnetic field B_0 and the polarization of the laser E_0.
- only the component of the radiofrequency field B_1 orthogonal to the magnetic field B_0 actually induces resonating transitions between Zeeman sublevels.
- for a linearly polarized pumping beam, the amplitudes of the resonance signals used for the magnetic field B_0 measurement reach an extremum when the polarization direction E_0 is perpendicular to the magnetic field B_0.

We have finally chosen to control the beam polarization direction through a rotation of a polarizer placed in front of the ^{4}He cell and we have also designed the radiofrequency excitation coils so that the resulting radiofrequency field is parallel to the linear polarizer: whatever the relative orientation of the sensor with respect to the magnetic field direction, both polarisation E_0 and radiofrequency field B_1 directions can always be adjusted perpendicularly to the static field B_0. The resulting magnetometer is thus perfectly isotropic.

The final instrument assembly consists of an electronic box (Digital Processing Unit) installed within the platform and a sensor mounted at the tip of the boom (to minimize the magnetic perturbations from the satellite) connected to the electronic box by a bundle of optical fibers and electrical cables (harness). As a cold redundancy has been required for the instrument, a specific sensor bracket has been designed to mechanically interface two identical sensors with the satellite boom, each sensor being connected to a dedicated DPU. Both ASM sensor and ASM DPU functional architectures are depicted on Fig. 2 .

The ASM sensor is made of:

- a PEEK based rotor comprising:
  - the ^{4}He cell containing a low pressure helium gas which is the sensing part of the sensor
  - HF electrodes used to apply an electric discharge to the ^{4}He gas thus transferring some of the atoms from the 1^1S_0 ground state to the 2^3S_1 metastable level
  - RF coils used to apply a RF field to the excited helium atoms to induce the magnetic resonance between the Zeeman sublevels of the 2^3S_1 metastable level
  - a linear polarizer whose rotation ensures optimal pumping conditions of the ^{4}He gas
  - a retro reflector used to reflect the laser light back through the cell to the DPU

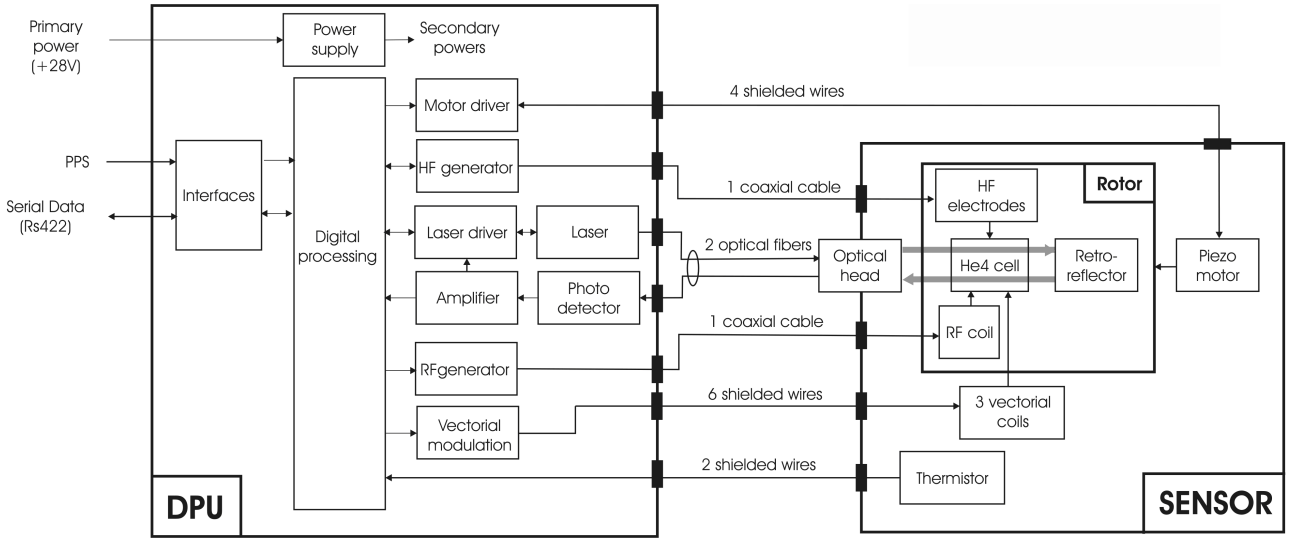

Fig. 2. ASM functional architecture

- a PEEK based stator comprising :
  - the totally amagnetic piezoelectric motor used to drive the rotor and so keep a constant θ_F = 90° angle between both polarization and RF field directions and the ambient magnetic field
  - rotating transformers to ensure contactless electrical connections to the HF electrodes and RF coils integrated on the rotor
  - a temperature sensor probe
  - three orthogonal vector coils for the vector mode.

The ASM DPU is divided in two stacked modules:

- the first module consists of the optical part of the DPU (a 1083 nm laser synthesis and the optical interface with the sensor) and the primary to secondary power DC-DC converters. This module can be divided into three sub-systems:
  - an electronic card delivering the secondary voltages (±5V, +3,3V) to all the electronic circuits of the DPU.
  - the laser source which delivers optical power to the sensor including a Laser Fiber Assembly using a fiber Bragg grating laser whose wavelength can be tuned on the D_0 transition (2^3S_1 - 2^3P_0, $\lambda \sim 1083$ nm) thanks to a piezoelectric actuator.
  - the optical interface circuit including the pump laser diode, photodiodes and their dedicated low noise amplifiers and the electrical bonding for the piezoelectric actuator.
- the second module contains the main digital and analog circuits, and regroups most of the electrical interfaces with the sensor and the satellite :
  - the main digital core
  - electrical interfaces and a test socket
  - the different data acquisition and signal processing modules
  - the RF, HF, laser, piezoelectric motor and vector mode drivers

Since this CEA-LETI magnetometer technology will be launched and operated in space for the first time, all ASM elements have been validated with respect to the environment specifications of the SWARM mission. A number of ASM specific and complex components such as the fiber Bragg grating laser have been successfully developed and qualified. A picture of the final ASM components including the ASM sensor assembly, the ASM DPU and the optical and electrical harnesses is given in Fig. 3. The different ASM flight models are currently being manufactured and will be available for the SWARM satellites integration in 2010.

Fig. 3. ASM sensor assembly and ASM DPU

ASM PERFORMANCES

ASM scalar performances

Compared to the Overhauser based scalar sensors previously used for the Ørsted and CHAMP missions [4], the scalar resolution has been enhanced to 1 pT/√Hz and the scalar bandwidth previously limited to a few tenths of Hz can be increased up to 300 Hz. For the SWARM mission, the scalar bandwidth has been tuned to 100 Hz so that vector modulations frequencies can be adjusted over a large frequency range below 100 Hz. The ASM scalar bandwidth and resolution are illustrated on Fig. 4.

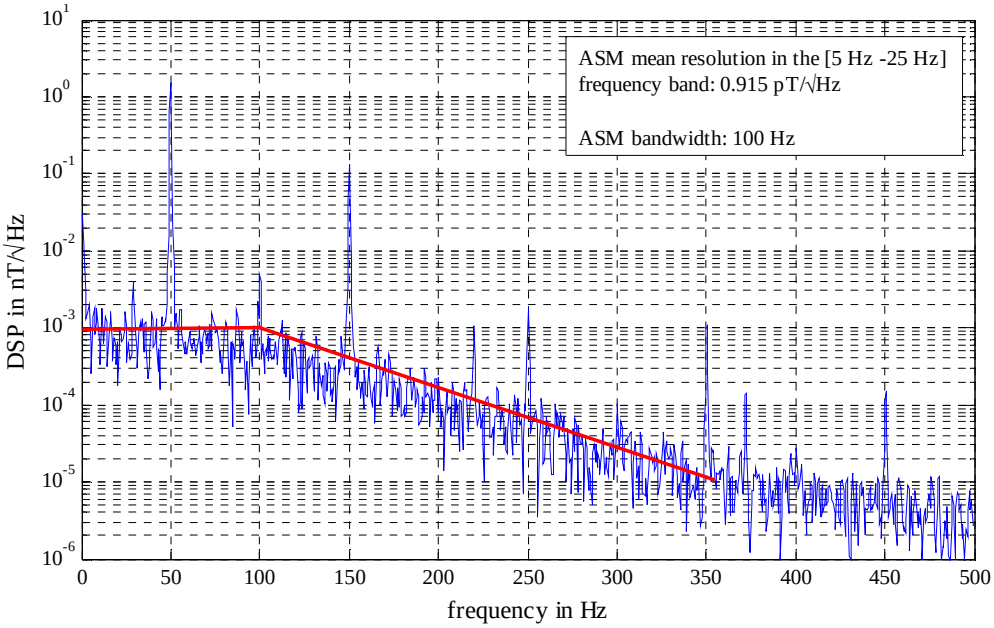

Fig. 4. ASM scalar bandwidth and resolution

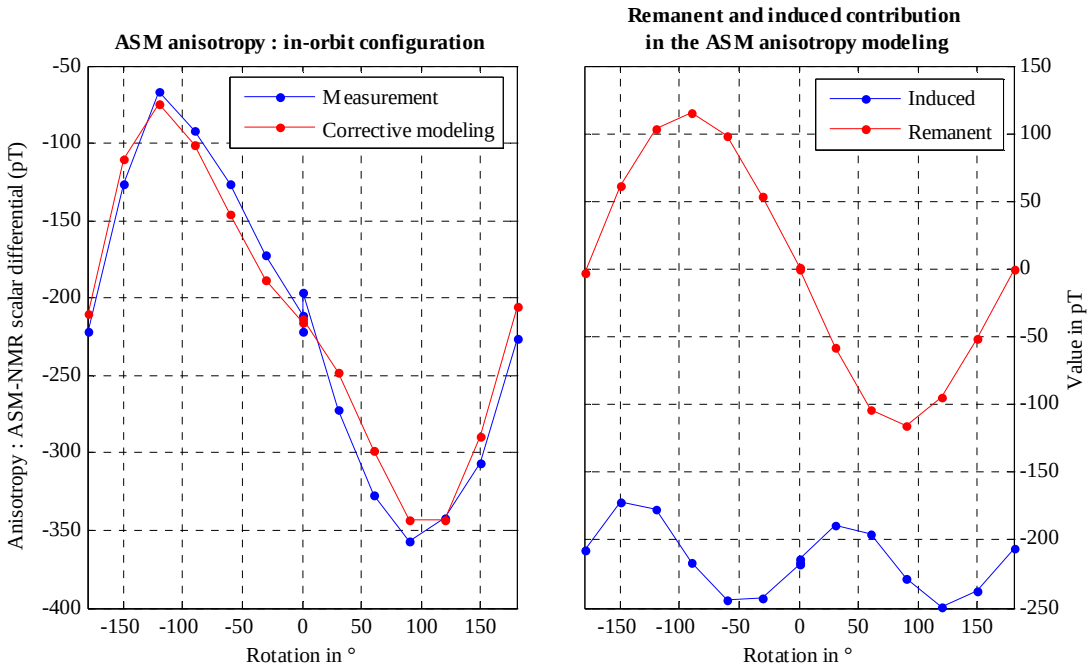

Fig. 5. ASM anisotropy and associated Algo1B corrective modeling for the in-orbit configuration of the ASM sensor

The specific ASM errors affecting the scalar magnetic field measurement have been identified and characterized:

- the ASM sensor anisotropy,
- the vector modulations aliasing (in vector mode only),
- the Bloch-Siegert effect [5],
- the measurement datation error,
- the Pulse Per Second (PPS) time reference accuracy

For example the ASM sensor assembly has been characterized and an associated corrective model including both remanent and induced magnetic field contributions has been derived: the results of this characterization for the in-orbit ASM sensor assembly configuration is given on Fig. 5. We could see that the main contribution on the ASM sensor assembly anisotropy is given by a induced magnetic field contribution: although the sensor assembly has been designed and realized with amagnetic materials such as PEEK, their magnetic susceptibilities are not equal to zero (magnetic susceptibilities χ range between 10^{-6} and 10^{-5} SI).

The measured and calculated maximum error contributions are given in the following table. Corresponding maximum remaining errors after the ASM level 1B algorithms corrections are also given and a final maximum quadratic remaining error on the absolute accuracy about 50 pT is demonstrated. Additional error contributions such as the satellite magnetic moment and the magnetocouplers effect will be corrected at satellite level with the SWARM satellite level 1B algorithms.

Error type	**Bloch-Siegert error**	**Vector aliasing**	**ASM in-orbit anisotropy**	**PPS precision** (5.10-7 x B_0) (worst case)	**Datation** (1 ms x 30 nT/s) (worst case)
ASM error before correction	55 pT (@ 46 µT)	23 pT (@ 46 µT)	120 pT	32,5 pT (@ 65 µT)	30 pT
Remaining error after ASM level 1B algorithm correction	< 5 pT	< 5 pT	< 25 pT	32,5 pT (@ 65 µT) (system error, not corrected in the level 1B algorithms)	30 pT (instrument error, not corrected in the level 1B algorithms)

Table 1. ASM errors contributions on the scalar measurement (resulting maximum quadratic error σ_{max}: 50 pT)

ASM vector performances

While the main objective of the ASM is to provide high resolution scalar measurements for the calibration of the VFM sensor, the ASM is also able to provide in addition vector measurements from its own with a resolution in the nT/√Hz range [2], a vector measurement bandwidth set to 0.4 Hz and a vector absolute precision of about 1 nT.

To be properly used, the vector mode has to pass a calibration process detailed in [2], and derived calibration parameters will be used in the ASM vector level 1B algorithm. This is illustrated on Fig. 6 corresponding to the measurements taken during a 3D calibration spiral applied on the ASM sensor, resulting in a preliminary scalar residual lower than +/- 2 nT peak-to-peak.

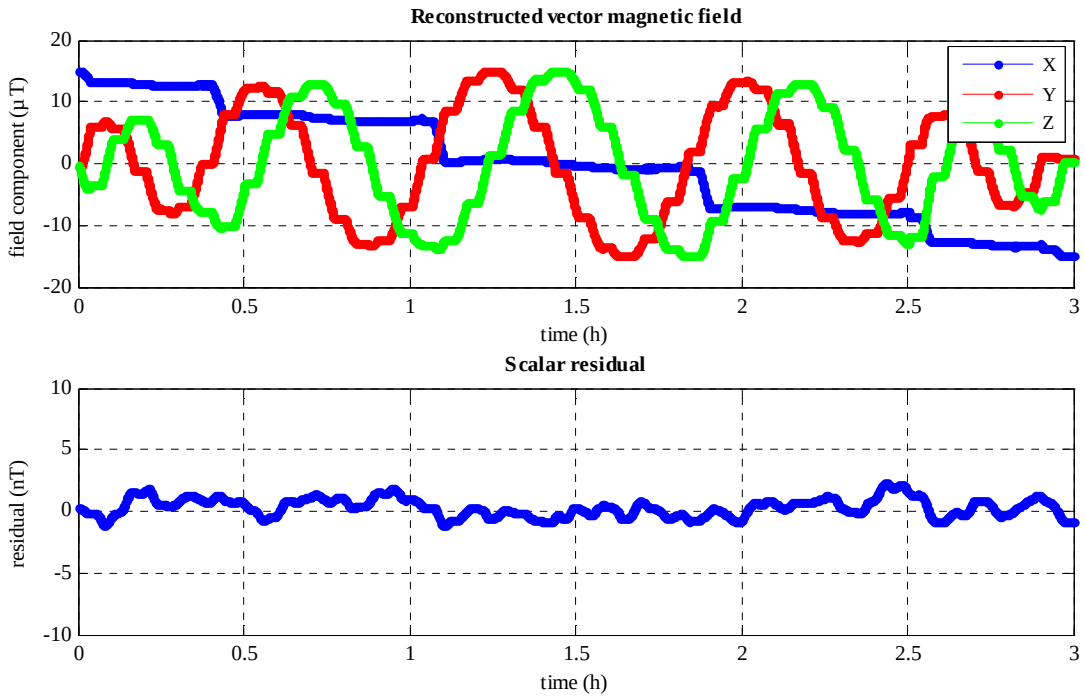

Fig. 6: preliminary ASM vector calibration (15 µT spiral)

CONCLUSION

The CEA-LETI has successfully designed and realized an optically pumped ^{4}He magnetometer which provides absolute scalar magnetic field measurements with a 1 pT/√Hz resolution over a DC to 100 Hz bandwidth. Its final corrected scalar accuracy is better than 50 pT. The ASM instrument is also able to provide vector field measurements with an intrinsic 1 nT/√Hz resolution and a 0.4 Hz bandwidth. All ASM components have been successfully qualified with respect to the environment and performances specifications of the SWARM mission. The different ASM flight models are currently being manufactured and will be delivered for their integration in the SWARM satellites in 2010.

REFERENCES

[1] Colegrove, F. D. and L. D. Schearer, "Optical pumping of helium in the 3S1metastable state", *Physical Review*, 119, 680–690, 1961.
[2] O. Gravrand, A. Khokhlov, J.L. Le Mouël, and J. M. Léger, "On the calibration of a vectorial 4He pumped magnetometer," *Earth Planets Space*, 53, 2001, pp. 949–958.
[3] Shifrin V.Y. and al," Experimental Determination of the Gyromagnetic Ratio of the Helium-4 Atom in Terms of that of the Helium-3 Nucleus", *IEEE Transactions on Instrumentation and Measurement*, Vol.46, No. 2, 1997, pp. 97-100.

[4] D. Duret, J.M. Léger, M. Francès, J.Bonzom and F. Alcouffe, “Performances of the OVH Magnetometer For The Danish Oersted Satellite”, *IEEE Transactions On Magnetics*, Vol. 32, No. 5, 1996, pp. 4935-4937.
[5] J.A. Hermann and S. Swain, “Bloch-Siegert shifts and multi-quantum transitions in spin-one systems”, *J. Phys. B: Atom. Molec. Phys.*, Vol 10, No. 11, 1977, pp. 2111-2123.